Technical University of Denmark

DTU

Surface roughness model for LINCOM

Astrup, Poul; Jensen, N.O.; Mikkelsen, Torben Krogh

Link back to DTU Orbit

DTU Library
Technical Information Center of Denmark

RISØ

DK9601519

Surface Roughness Model for LINCOM

Poul Astrup, Niels Otto Jensen, Torben Mikkelsen

Surface Roughness Model for LINCOM

Poul Astrup, Niels Otto Jensen, Torben Mikkelsen

Abstract

The LINCOM model for neutrally stable flow over complex terrain, developed in 1986 by Troen and de Bass [13], has been extended to also respond to variations in surface roughness. The extension is based on the assumption that close to the ground the flow is in equilibrium with the local surface roughness, and on a model for the vertical extent of this equilibrium zone.

LINCOM is based on an analytical solution in Fourier space to a set of linear equations derived from the normal nonlinear mass and momentum equations for fluid flow. The linear equations describe the perturbations in velocity and pressure that the real terrain induces in an equilibrium flow corresponding to a flat terrain with uniform surface roughness. The perturbations caused by gradients in ground elevation and surface roughness are determined separately and summed as a first order approximation to the combined perturbation.

DISCLAIMER

Portions of this document may be illegible
in electronic image products. Images are
produced from the best available original
document.

Contents

Acknowledgements

Nomenclature

latin:

a	± 1 $(= \text{sign}[kU + mV])$
a	function
a	constant
A	function
A	area [m^2]
c_1	fitting parameter of order 1
c_2	fitting parameter of order 1
C	helping parameter
e	unit vector, $(\cos\theta, \sin\theta, 0)$
f	correction factor
F	Fourier transform
g	gravity [m/s^2]
h	surface elevation
k	wavenumber in x-direction [rad/m]
K	effective kinematic viscosity [m^2/s]
l	inner scale length [m]
$\ln$	natural logarithm
L	outer scale length [m]
m	wavenumber in y-direction [rad/m]
N_x	number of nodes in x-direction
p	pressure [N/m^2]
p	Fourier space pressure perturbation [m^4/s^2]
$\widetilde{p}$	real space pressure perturbation [m^2/s^2]
$\bar{p}$	mean pressure [N/m^2]
P	background pressure field [N/m^2]
t	time [s]
u	Fourier space velocity perturbation component [m^3/s]
$\widetilde{u}$	real space velocity perturbation component [m/s]
u_*	friction velocity perturbation [m/s]
U	background velocity component [m/s]
U_*	local friction velocity [m/s]
U_{*0}	friction velocity corresponding to background flow [m/s]
v	Fourier space velocity perturbation component [m^3/s]
$\widetilde{v}$	real space velocity perturbation component [m/s]
v	real space velocity field [m/s]
$\bar{v}$	real space mean velocity field [m/s]
$\widetilde{v}$	real space velocity perturbation field [m/s]
V	background velocity component [m/s]
V	background velocity field [m/s]
w	Fourier space velocity perturbation component [m^3/s]
$\widetilde{w}$	real space velocity perturbation component [m/s]
x	coordinate [m]
X	x-direction size of modelled area [m]
y	coordinate [m]
z	coordinate, height [m]
z_0	mean surface roughness height [m]
z_1	local surface roughness height [m]

z_r	upper limit for local equilibrium [m]
0	zero vector
0	zero tensor

greek:

α	exponent
η	z_1/z_0
θ	angle between x-axis and background velocity vector
κ	von Karman constant ≈ 0.4
λ	wavenumber [m^{-1}]
μ	dynamic viscosity [kg m^{-1}s^{-1}]
ν	kinematic viscosity [m^{2}s^{-1}]
ρ	density [kg/m^3]

subscript:

0	at height 0
1	outer solution
2	inner solution
l	at height l
L	at height L
z	at height z

superscript:

T	transposed
$'$	turbulent fluctuation
$-$	real space mean value
$\sim$	real space perturbation parameter

1 Introduction

For the last decade wind flow models have been developed and evaluated within Risø's Department of Meteorology and Wind Energy, partly for use with wind energy applications, and partly to generate flow fields as input to dispersion calculations with our puff dispersion model Rimpuff [8].

Within the concept of linearized flow models Troen and de Baas [13] in 1986 developed a model for neutrally stable flow over complex terrain – later named LINCOM – and in 1994 Santabàrbara et al [10] extended this model to include the gravitational forces caused by departure from neutral stability.
In the present work the neutrally stable model is extended to respond to surface roughness variations.

The linear equations – derived from the normal nonlinear mass and momentum equations for fluid flow – describe the perturbations in velocity and pressure, which the real terrain induces in a background flow in equilibrium with a flat terrain with uniform surface roughness.
Taking the Fourier transform over the two horizontal coordinates, the differential x and y dependencies reduce to scalar dependencies in the corresponding wavenumbers k and m, leaving a differential dependence in the z coordinate only. With proper approximations the resulting equations have analytical solutions, and the LINCOM models are all based on these.

Solving for perturbations the final solution can to first order be taken as the sum of perturbations caused by different mechanisms, and the inclusion of surface roughness is the inclusion of a solution fulfilling a set of boundary conditions derived from the hypothesis that the near ground flow is in equilibrium with the local surface roughness.

The final flow field is obtained by adding the sum of perturbations to the background flow.

While only the roughness model is new, described in chapter 6, all the basics of the LINCOM model are for consistency reasons given in the following, chapters 2 to 5, here based upon Troen and de Baas [13], Troen [12] and Santabàrbara et al [10],

2 The background flow

The background flow is the equilibrium flow over a flat terrain with a uniform roughness height z_0. Using mixing length closure, the effective diffusivity K increases linearly with height and the velocity profile is logarithmic:

$$K = \kappa U_{*0} z \tag{1}$$

$$V = e \frac{U_{*0}}{\kappa} \ln \frac{z}{z_0} \tag{2}$$

Here

$$e = (\cos\theta, \sin\theta, 0) \qquad (3)$$

is the unit vector in the direction of the background flow.

3 Basic equations

The starting point is the differential form of the mass and momentum equations, the latter in the form of the Navier-Stokes equation. Temperature is not solved for in neutral LINCOM so the energy equation is omitted. In vector notation it can be written [1]:

$$\frac{\partial \rho}{\partial t} + \nabla \cdot (\rho v) = 0 \qquad (4)$$

$$\frac{\partial}{\partial t}(\rho v) + \nabla \cdot (\rho\, vv) = \rho g - \nabla p + \nabla \cdot [\mu(\nabla v + \nabla v^T)] - \tfrac{2}{3}\nabla(\mu\nabla \cdot v) \qquad (5)$$

Assuming steady state and incompressibility it reduces to

$$\nabla \cdot v = 0 \qquad (6)$$

$$v \cdot \nabla v = g - \frac{\nabla p}{\rho} + \nabla \cdot (\nu \nabla v) \qquad (7)$$

Introducing Reynolds decomposition, overbar $^-$ designating mean and $'$ fluctuation, this becomes

$$\nabla \cdot \overline{v} = 0 \qquad (8)$$

$$\overline{v} \cdot \nabla \overline{v} = g - \frac{\nabla \overline{p}}{\rho} + \nabla \cdot (\nu \nabla \overline{v}) - \nabla \cdot \overline{v'v'} \qquad (9)$$

In normal turbulent flow the Reynolds stress $-\nabla \cdot \overline{v'v'}$ is much larger than the molecular stress $\nabla \cdot (\nu \nabla \overline{v})$ and the sum is here modelled as

$$\nabla \cdot (\nu \nabla \overline{v}) - \nabla \cdot \overline{v'v'} = \nabla \cdot (K \nabla \overline{v}) \qquad (10)$$

where K is the effective turbulent kinematic viscosity.

Now splitting both of $\overline{v}$ and $\overline{p}$ into a 'constant' field and a perturbation field

$$\overline{v} = V + \widetilde{v} \qquad (11)$$
$$\overline{p} = P + \widetilde{p} \qquad (12)$$

where the 'constant' fields obey

$$\nabla \cdot V = 0 \qquad (13)$$
$$\nabla V = \mathbf{0} \qquad (14)$$
$$\nabla P \equiv \rho g \qquad (15)$$

one gets from the mass and momentum equations

$$\nabla \cdot \widetilde{v} = 0 \qquad (16)$$

$$(V + \widetilde{v}) \cdot \nabla \widetilde{v} = -\frac{\nabla \widetilde{p}}{\rho} + \nabla \cdot (K \nabla \widetilde{v}) \qquad (17)$$

Now the real hard assumption is that $V \gg \widetilde{v}$ so that eq. 17 can be reduced to

$$V \cdot \nabla \widetilde{v} \;=\; -\frac{\nabla \widetilde{p}}{\rho} + \nabla \cdot (K \nabla \widetilde{v}) \tag{18}$$

whereby eqs. 16 and 18 forms a set of linear equations in $\widetilde{v}$ and $\widetilde{p}$. This set is further reduced by assuming K constant and by assuming the horizontal diffusion to be negligible as compared to the convection. Having $(U, V, 0)$ designating the x, y, z components of the 'constant' velocity field V, and $(\widetilde{u}, \widetilde{v}, \widetilde{w})$ the components of the velocity perturbation vector $\widetilde{v}$, we arrive at the following set of linear equations

$$U \frac{\partial \widetilde{u}}{\partial x} + V \frac{\partial \widetilde{u}}{\partial y} \;=\; -\frac{\partial}{\partial x}\frac{\widetilde{p}}{\rho} + K \frac{\partial^2 \widetilde{u}}{\partial z^2} \tag{19}$$

$$U \frac{\partial \widetilde{v}}{\partial x} + V \frac{\partial \widetilde{v}}{\partial y} \;=\; -\frac{\partial}{\partial y}\frac{\widetilde{p}}{\rho} + K \frac{\partial^2 \widetilde{v}}{\partial z^2} \tag{20}$$

$$U \frac{\partial \widetilde{w}}{\partial x} + V \frac{\partial \widetilde{w}}{\partial y} \;=\; -\frac{\partial}{\partial z}\frac{\widetilde{p}}{\rho} + K \frac{\partial^2 \widetilde{w}}{\partial z^2} \tag{21}$$

$$\frac{\partial \widetilde{u}}{\partial x} + \frac{\partial \widetilde{v}}{\partial y} + \frac{\partial \widetilde{w}}{\partial z} \;=\; 0 \tag{22}$$

where the mass equation is now the bottom one.

4 Solution method

The solution method is spectral ie the dependent variables are Fourier transformed and the mass and momentum equations expressed for these. A Fourier transform pair is normally defined as

$$a(\lambda) \;=\; \int_{-\infty}^{\infty} \widetilde{a}(x)\, e^{2\pi i x \lambda}\, dx \;=\; F[\widetilde{a}(x)] \tag{23}$$

$$\widetilde{a}(x) \;=\; \int_{-\infty}^{\infty} a(\lambda)\, e^{-2\pi i x \lambda}\, d\lambda \;=\; F^{-1}[a(\lambda)] \tag{24}$$

where λ is a wavenumber ie the number of waves per unit length. By the variable transformation

$$k \;=\; -2\pi\lambda \tag{25}$$
$$dk \;=\; -2\pi\, d\lambda \tag{26}$$
$$A(k) \;=\; a(\lambda) \;=\; a(-k/2\pi) \tag{27}$$

where then k is an angular wavenumber measured in radians per unit length, the transform can be written

$$A(k) \;=\; \int_{-\infty}^{\infty} \widetilde{a}(x)\, e^{-i k x}\, dx \tag{28}$$

$$\widetilde{a}(x) \;=\; \frac{1}{2\pi} \int_{-\infty}^{\infty} A(k)\, e^{i k x}\, dk \tag{29}$$

Letting u, v, w, p be the 2D Fourier space equivalents to $\widetilde{u}, \widetilde{v}, \widetilde{w}, \widetilde{p}/\rho$ we get the transformation pair eg for $\widetilde{u}(x, y, z), u(k, m, z)$:

$$
\begin{aligned}
u(k, m, z) &= \iint_{-\infty}^{\infty} \widetilde{u}(x, y, z)\, e^{-ikx - imy}\, dx\, dy \\[2mm]
&= F[\widetilde{u}(x, y, z)] \tag{30}
\end{aligned}
$$

$$
\begin{aligned}
\widetilde{u}(x, y, z) &= \frac{1}{4\pi^2} \iint_{-\infty}^{\infty} u(k, m, z)\, e^{ikx + imy}\, dk\, dm \\[2mm]
&= F^{-1}[u(k, m, z)] \tag{31}
\end{aligned}
$$

Thereby

$$
\frac{\partial \widetilde{u}}{\partial x} = F^{-1}[ik\, u(k, m, z)] \tag{32}
$$

$$
\frac{\partial \widetilde{u}}{\partial y} = F^{-1}[im\, u(k, m, z)] \tag{33}
$$

$$
\frac{\partial \widetilde{u}}{\partial z} = \frac{\partial F^{-1}[u(k, m, z)]}{\partial z} = F^{-1}\left[\frac{\partial u(k, m, z)}{\partial z}\right] \tag{34}
$$

The x-momentum equation eq. 19 can then be written

$$
U F^{-1}[iku] + V F^{-1}[imu] = -F^{-1}[ikp] + K F^{-1}\left[\frac{\partial^2 u}{\partial z^2}\right] \tag{35}
$$

With U, V, K being constant insertion of F^{-1}, eq. 31, gives

$$
\iint_{-\infty}^{\infty} \left[(ikU + imV)\, u + ikp - K\, \frac{\partial^2 u}{\partial z^2}\right] e^{ikx + imy}\, dk\, dm = 0 \tag{36}
$$

which is only generally valid for the integrand being zero. As $e^{ikx + imy} \neq 0$ the expression inside the parentheses must equal zero. The equations in Fourier space corresponding to eqs. 19 to 22 then become

$$
(ikU + imV)\, u + ikp - K\, \frac{\partial^2 u}{\partial z^2} = 0 \tag{37}
$$

$$
(ikU + imV)\, v + imp - K\, \frac{\partial^2 v}{\partial z^2} = 0 \tag{38}
$$

$$
(ikU + imV)\, w + \frac{\partial p}{\partial z} - K\, \frac{\partial^2 w}{\partial z^2} = 0 \tag{39}
$$

$$
iku + imv + \frac{\partial w}{\partial z} = 0 \tag{40}
$$

4.1 Generic Fourier space solution

The solutions to such linear differential equations with constant coefficients are functions of the form

$$
a = a_0\, e^{\alpha z} \tag{41}
$$

Introducing this into eqs. 37 to 40 reduces these to the scalar equations

$$(ikU + imV - K\alpha^2)u + ikp = 0 \tag{42}$$
$$(ikU + imV - K\alpha^2)v + imp = 0 \tag{43}$$
$$(ikU + imV - K\alpha^2)w + \alpha p = 0 \tag{44}$$
$$iku + imv + \alpha w = 0 \tag{45}$$

or in matrix form with

$$C \equiv ikU + imV - K\alpha^2 \tag{46}$$

$$\begin{pmatrix} C & 0 & 0 & ik \\ 0 & C & 0 & im \\ 0 & 0 & C & \alpha \\ ik & im & \alpha & 0 \end{pmatrix} \begin{pmatrix} u \\ v \\ w \\ p \end{pmatrix} = \begin{pmatrix} 0 \\ 0 \\ 0 \\ 0 \end{pmatrix} \tag{47}$$

This obviously has the uninteresting solution $(u, v, w, p) = 0$, so interesting solutions is only found when the matrix has zero determinant. This is obtained for

$$C^2(k^2 + m^2 - \alpha^2) = 0 \tag{48}$$

from where the applicable α's are found:

$$\alpha = \begin{cases} \pm\sqrt{k^2 + m^2} \\ \pm\sqrt{\dfrac{i(kU + mV)}{K}} \end{cases} \tag{49}$$

For the solutions to stay limited for increasing z only α's with a negative real part have reason. This limits α to

$$\alpha = \begin{cases} -\sqrt{k^2 + m^2} \\ -\sqrt{\dfrac{|kU + mV|}{2K}} * \begin{cases} 1 + i & \text{for} \quad kU + mV \geq 0 \\ 1 - i & \text{for} \quad kU + mV < 0 \end{cases} \end{cases} \tag{50}$$

Defining two length scales and the number a as

$$L \equiv \frac{1}{\sqrt{k^2 + m^2}} \tag{51}$$

$$l \equiv \sqrt{\frac{K}{|kU + mV|}} \tag{52}$$

$$a \equiv \text{sign}[kU + mV] \tag{53}$$

the α's are expressed

$$\alpha = \begin{cases} -\dfrac{1}{L} = \alpha_1 \\ -\dfrac{1 + ai}{l\sqrt{2}} = \alpha_2 \end{cases} \tag{54}$$

The solution corresponding to α_1 is called the outer solution and that corresponding to α_2 is called the inner solution. As the equation system is linear the final solution is found as the sum of the outer and inner solutions.

$$
\begin{pmatrix} u \\ v \\ w \\ p \end{pmatrix} = \begin{pmatrix} u_1 \\ v_1 \\ w_1 \\ p_1 \end{pmatrix} + \begin{pmatrix} u_2 \\ v_2 \\ w_2 \\ p_2 \end{pmatrix}
$$

$$
= \begin{pmatrix} u_{10} \\ v_{10} \\ w_{10} \\ p_{10} \end{pmatrix} e^{-\frac{z}{L}} + \begin{pmatrix} u_{20} \\ v_{20} \\ w_{20} \\ p_{20} \end{pmatrix} e^{-\frac{1+ai}{\sqrt{2}}\frac{z}{l}} \tag{55}
$$

The length scales L and l correspond to the scales defined by Jackson and Hunt [4] for their outer and inner layers and relate to each other exactly as those. Thus L is a horizontal scale of the perturbation and l is a scale for the height below which the perturbation is viscous.

For the outer solution eq. 47 gives the following relations between the elements of the arbitrary constants vector:

$$
p_{10} = \frac{-Cw_{10}}{\alpha_1} = CLw_{10} \tag{56}
$$

$$
u_{10} = \frac{-ikp_{10}}{C} = -ikLw_{10} \tag{57}
$$

$$
v_{10} = \frac{-imp_{10}}{C} = -imLw_{10} \tag{58}
$$

The inner solution corresponds to $C = 0$ and eq. 47 gives the relations

$$
iku_{20} + imv_{20} - \frac{1+ai}{l\sqrt{2}}w_{20} = 0 \tag{59}
$$

$$
p_{20} = 0 \tag{60}
$$

So the outer solution needs one boundary condition to fix its arbitrary constants and the inner solution needs two.

The outer solution is inviscid and gives the pressure distribution while the inner solution is viscous and doesn't add to the pressure.

4.1.1 Determination of l

Despite the assumptions $\nabla V = 0$ and K constant used in the derivation of the final set of equations, U, V and K, as they enter the solution through the expression for l, eq. 52, are taken from the background flow values at the scaled heights lc_1 and lc_2 where c_1 and c_2 are fitting parameters of the order of 1, Troen and de Baas [13].

$$
U = \cos\theta \frac{U_{*0}}{\kappa} \ln\frac{lc_1}{z_0} \tag{61}
$$

$$V = \sin\theta \frac{U_{*0}}{\kappa} \ln\frac{lc_1}{z_0} \tag{62}$$

$$K = \kappa U_{*0} l c_2 \tag{63}$$

A transcendent equation for l emerges which in the form

$$\frac{lc_1}{z_0} \ln\frac{lc_1}{z_0} = \frac{c_1 c_2}{z_0} \frac{\kappa^2}{|k\cos\theta + m\sin\theta|} \tag{64}$$

is easily solved by Newton-Raphson iteration in the variable lc_1/z_0 when starting at

$$\frac{lc_1}{z_0}\bigg|_{\text{start}} = \left[\frac{c_1 c_2}{z_0} \frac{\kappa^2}{|k\cos\theta + m\sin\theta|} \frac{1}{1.78}\right]^{\frac{1}{1.2}} \tag{65}$$

4.2 Specific solution

The perturbations for a specific problem are obtained by applying the boundary conditions for the problem – one for the outer and two for the inner solution – thereby obtaining the specific values for the arbitrary constants vectors, inserting these in eq. 55 and Fourier transforming to real space according to eq. 31.

The final flow is then found by adding the perturbation to the background flow.

5 Flow over hills

For flow over hills the boundary condition is based upon the fact that close to the ground the flow is parallel to this. Troen and de Baas [13] use scale arguments to reduce this to a condition for the outer solution only, a "full slip" condition reading:

$$\begin{aligned} \tilde{w}_{1,z=0} &= \mathbf{V} \cdot \nabla \tilde{h} \\ &= U\frac{d\tilde{h}}{dx} + V\frac{d\tilde{h}}{dy} \end{aligned} \tag{66}$$

where $\tilde{h}$ is the ground surface elevation as function of x, y. Thereby the actual height is disregarded, only the slope counts, and z becomes a kind of height above ground, although no real coordinate transformation is carried out.
Transforming to Fourier space applying the normal assumptions for this step, eq. 66 becomes

$$w_{10} = -i(kU + mV)h \tag{67}$$

The U and V used here are taken from the background flow at a height corresponding to the outer length scale as given by eq. 51. This models that low wavenumber perturbations are influenced from larger heights and penetrates to larger heights, than small wavenumber perturbations. u_{10}, v_{10}, and p_{10} follow from eqs. 56 to 58.

The inner solution is used to force the u and v perturbations to zero at the ground by setting

$$u_{20} = -u_{10} \tag{68}$$
$$v_{20} = -v_{10} \tag{69}$$

w_{20} follows from eq. 59.

5.1 Simpler approach

In a somewhat simpler approach Troen [12] and Troen and Petersen [14] skips the inner solution and applies a correction factor to the perturbation velocity of the outer solution reading:

$$f = \begin{cases} \dfrac{|V_L|}{|V_z|} & \text{for } z > l \\[2ex] \dfrac{|V_L||V_z|}{|V_l|^2} & \text{for } z \le l \end{cases} \tag{70}$$

Here V is again the background flow, eq. 2, and the subscripts indicate the heights at which it is determined. And in stead of the iterative procedure of chapter 4.1.1 the length scale l is taken from Jensen et al [5]:

$$l = 0.3 z_0^{0.33} L^{0.67} \tag{71}$$

The reason for the factor is due to Troen and Petersen [14] that the outer solution underpredicts the speedup at heights around l, where it is maximum. Although explained somewhat differently, Troen [12] arrives at the factor used for $z > l$ by neglecting the diffusivity term of the parameter C, eq. 46, and by basing this on velocities at different heights when used in eq. 56 and in eqs. 57 and 58. In eq. 56 it is based on the velocity at height L and in eqs. 57 and 58 it is based on the velocity at the actual height z. Thereby eg for u_{10}:

$$u_{10} = -ikLw_{10}\frac{C_L}{C_z}$$

$$= -ikLw_{10}\frac{|V_L|}{|V_z|} \tag{72}$$

For $z \le l$ the factor is proportional to $|V_z|$, matching that at $z = l$, and thus making the perturbation a continuous function approaching zero for $z \to z_0$.

6 Surface roughness

Boundary equation

Many models make use of a constant-flux layer close to the ground for describing the influence of the ground on the conditions away from the ground, [15]. In line with this the boundary condition describing the influence of surface roughness is based upon the assumption, that close to the ground the flow is in equilibrium with the local surface roughness, ie below some height z_r the flux of momentum is invariant with height and the vertical profile of the horizontal velocity is logarithmic:

$$\overline{v} = e \frac{U_*}{\kappa} \ln \frac{z}{z_1} \tag{73}$$

Here U_* and z_1 are the local values of friction velocity and roughness height.
As explained in chapter 2 the background flow is in equilibrium with the roughness height z_0, which in the present context has to equal the mean logarithmic roughness height of the area of interest and gets defined as:

$$\ln z_0 \equiv \frac{1}{A} \int_A \ln z_1 \, dA \tag{74}$$

Specifying

$$\eta \equiv \frac{z_1}{z_0} \tag{75}$$

we find

$$\frac{1}{A} \int_A \ln \eta \, dA = 0 \tag{76}$$

Subtraction of the background flow, eq. 2, from the actual flow, eq. 73, gives the perturbation velocity $\widetilde{v}$ which is then expressed

$$\widetilde{v} = e \left(\frac{U_* - U_{*0}}{\kappa} \ln \frac{z}{z_0} - \frac{U_*}{\kappa} \ln \eta \right) \tag{77}$$

By defining

$$u_* \equiv U_* - U_{*0} \tag{78}$$

eq. 77 becomes

$$\widetilde{v} = e \left(\frac{u_*}{\kappa} \ln \frac{z}{z_0} - \frac{U_{*0} + u_*}{\kappa} \ln \eta \right) \tag{79}$$

The only z-dependent right side term is the logarithm for which reason the vertical profile of $\widetilde{v}$ is also logarithmic. The z-derivative becomes

$$\frac{\partial \widetilde{v}}{\partial z} = e \frac{u_*}{\kappa z} \tag{80}$$

As the boundary condition is needed in Fourier space, eq. 79 has to be Fourier transformed. The second term on the right hand side, however, includes a product of two x, y-dependent properties ie u_* and η, and the Fourier transform of a product is not a simple analytical function of the Fourier transforms of the factors. We therefore have to avoid the product. This is obtained by limiting also the stress perturbation to 1st order, ie by assuming $u_* \ll U_{*0}$ and eq. 79 can thereby be approximated as

$$\widetilde{v} = e \left(\frac{u_*}{\kappa} \ln \frac{z}{z_0} - \frac{U_{*0}}{\kappa} \ln \eta \right) \tag{81}$$

Insertion of eq. 80 and application of the Fourier transform gives

$$v = z \frac{\partial v}{\partial z} \ln \frac{z}{z_0} - e \frac{U_{*0}}{\kappa} F[\ln \eta] \tag{82}$$

and this describes the perturbation velocity in Fourier space and close to the ground, ie up to the above mentioned height z_r, below which equilibrium is assumed. So eq. 82 forms a boundary condition at $z = z_r$ for the velocity perturbation solution.

Velocity perturbation

Insertion of z_r into eq. 82 and splitting the vectors into their components gives two of the three sought boundary conditions:

$$u = z_r \frac{\partial u}{\partial z}\Big|_{z_r} \ln\frac{z_r}{z_0} - \cos\theta \frac{U_{*0}}{\kappa} F[\ln\eta] \qquad (83)$$

$$v = z_r \frac{\partial v}{\partial z}\Big|_{z_r} \ln\frac{z_r}{z_0} - \sin\theta \frac{U_{*0}}{\kappa} F[\ln\eta] \qquad (84)$$

An applicable third condition is $w = 0$ at $z = 0$, even though the real space final solution is not valid for $z < z_1$.

The boundary conditions can be applied to the total solution eqs. 55 to 60 directly or the two conditions from eqs. 83 and 84 can be applied to the inner solution fixing u_{20} and v_{20}, eq. 59 then fixing w_{20}, followed by the application of $w = 0$ at $z = 0$ to give $w_{10} = -w_{20}$. The latter option fixes the inner solution u_2, v_2 rather than the total solution u, v to the found boundary conditions and is the one preferred since the inner solution is the viscous solution and surface stress a viscous phenomenon.

The Fourier space boundary condition for u_2 is then from eqs. 83 and 41

$$u_{2,z_r} = z_r \frac{\partial u_2}{\partial z}\Big|_{z_r} \ln\frac{z_r}{z_0} - \frac{U_{*0}}{\kappa} \cos\theta\, F[\ln\eta]$$

$$= z_r \alpha_2 u_{2,z_r} \ln\frac{z_r}{z_0} - \frac{U_{*0}}{\kappa} \cos\theta\, F[\ln\eta] \qquad (85)$$

from where u_{2,z_r} is found. With eqs. 41 and 54 u_{20} and equivalently v_{20} are found as

$$u_{20} = -\frac{U_{*0}}{\kappa} \cos\theta\, F[\ln\eta] \left[1 + \frac{1+ai}{\sqrt{2}} \frac{z_r}{l} \ln\frac{z_r}{z_0}\right]^{-1} e^{\frac{1+ai}{\sqrt{2}}\frac{z_r}{l}} \qquad (86)$$

$$v_{20} = -\frac{U_{*0}}{\kappa} \sin\theta\, F[\ln\eta] \left[1 + \frac{1+ai}{\sqrt{2}} \frac{z_r}{l} \ln\frac{z_r}{z_0}\right]^{-1} e^{\frac{1+ai}{\sqrt{2}}\frac{z_r}{l}} \qquad (87)$$

w_{20} is found from eq. 59 giving

$$w_{20} = \frac{U_{*0}}{\kappa} \frac{F[\ln\eta]\,(k\cos\theta + m\sin\theta)}{\dfrac{i-a}{l\sqrt{2}}\left[1 + \dfrac{1+ai}{\sqrt{2}}\dfrac{z_r}{l}\ln\dfrac{z_r}{z_0}\right]} e^{\frac{1+ai}{\sqrt{2}}\frac{z_r}{l}} \qquad (88)$$

For the outer solution $w_{10} = -w_{20}$ as mentioned above, and u_{10}, v_{10}, p_{10} are given by eqs. 56, 57, 58.

Friction velocity

The friction velocity perturbation field u_* can be found from eq. 80 which being the z-derivative of the boundary condition equation is valid for $z \le z_r$. Fourier transforming the equation gives

$$e\, F[u_*] = \kappa z \frac{\partial v}{\partial z} \qquad (89)$$

The roughness boundary condition is applied to the inner solution at height $z = z_r$, and introducing this solution at the right hand side of eq. 89 leads to

16 Risø–R–900(EN)

$$F[u_*] = z_r U_{*0} F[\ln \eta] \frac{1+ai}{l\sqrt{2}} \left[1 + \frac{1+ai}{\sqrt{2}} \frac{z_r}{l} \ln \frac{z_r}{z_0} \right]^{-1} \qquad (90)$$

the inverse Fourier transform of which gives the u_* field. With eq. 78 the friction velocity field U_* is then obtained.

6.1 Determination of z_r

As seen from eqs. 86 to 90 the solution depends upon z_r, the height below which equilibrium is assumed. z_r cannot be determined analytically, it has to be found from sound reasoning combined with tests against data and for this purpose we have used the data of Bradley [3] and those of Peterson et al [9].

Bradley measured velocity profiles and surface friction as function of fetch downstream a smooth to rough transition and downstream a following rough to smooth transition. In the latter case the upstream fetch over rough surface was 22 m. The roughness heights corresponding to smooth and rough were 0.002 and 2.5 mm respectively. The calculations are correspondingly performed for a smooth/rough-/smooth surface the rough part being 22 m long.

Peterson et al measured velocity profiles as function of fetch downstream a smooth to rough transition, the smooth surface being water and the rough marshland. The fetch for the most downstream mast was 160 m and the roughness heights corresponding to smooth and rough were 0.35 and 6 mm respectively. The calculations are performed for a smooth/rough/smooth surface the rough part being 250 m long.

As used here z_r can have one of two forms: it can be a constant or it can be a function of the wavenumber.

Constant z_r

Walmsley et al [15] mention that z_r ought to be small compared to the inner scale length l and large compared to the mean friction height z_0 but they do get reasonable results for both velocity and stress perturbations using $z_r = z_0$ in their code MS3DJH/3R.

Choosing $z_r = z_0$ in LINCOM results in an overprediction of the velocity perturbations and zero stress perturbation. A bigger z_r gives more realistic results, but where $z_r = 10\, z_{1,max}$ gives reasonable results for the Bradley test, $z_r = 100\, z_{1,max}$ is needed for the Peterson test. And numerical problems arise furthermore when z_r/z doesn't stay low, z being the level for which the flow field is calculated.

Wavenumber dependent z_r

Several different dependencies of z_r upon wavenumber have been tried. To fulfill the condition of being small compared to l and large compared to z_0, the number $\sqrt{z_0 l}$ has been proposed by Belcher et al [2]. But in LINCOM this was found to overpredict the velocity perturbations. The best fit to the velocity data was found using the length scale originally proposed by Jensen et al [5] as a scale for l:

$$z_r = 0.3\, z_0^{0.33}\, L^{0.67} \qquad (91)$$

Figure 1 shows the relations between l, L, and this z_r for both the Bradley and the Peterson test cases. As they all go towards infinity for the wavenumber going to zero, this point has been omitted. Zero wavenumber, however, is treated in the calculations and with $z_r/l \to 0$ for $k,m \to 0,0$ it is seen from eqs. 86 to 88 to give
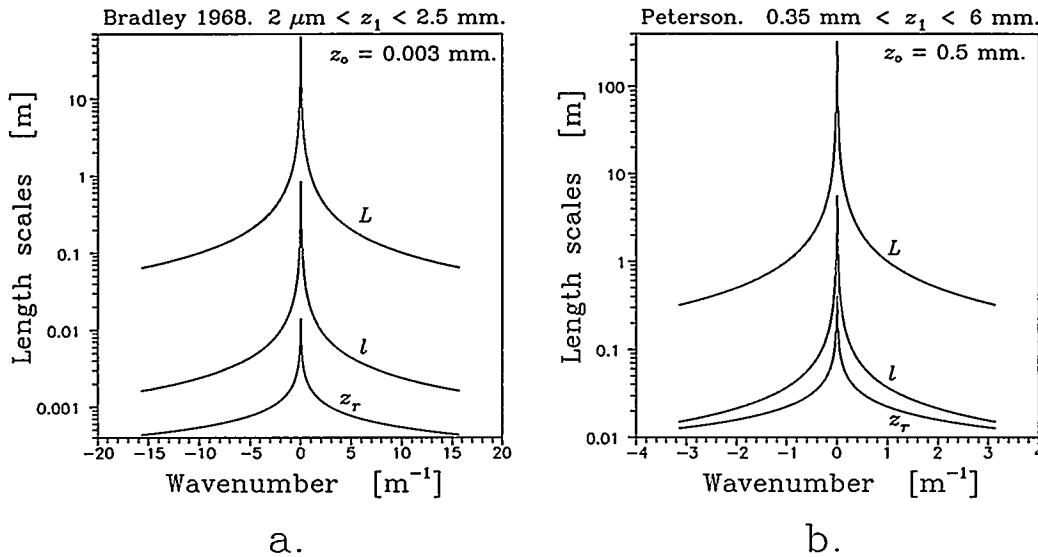
Figure 1. z_r, l, and L. a) Bradley case   b) Peterson case.

non vanishing terms. Minimum and maximum wavenumbers in the plots depend upon the number of nodes used, N_x, and the actual distance modelled, X:

$$k_{\min} = \pm 2\pi / X \tag{92}$$

$$k_{\max} = \pm N_x \pi / X \tag{93}$$

and equivalently for the y direction, which is absent, however, in these one dimensional test cases. For the Bradley case $N = 2048$ and $X = 409.6\,\mathrm{m}$ giving $k_{\min} = 0.0153\,\mathrm{m}^{-1}$ and $k_{\max} = 15.7\,\mathrm{m}^{-1}$, while for the Peterson case $N = 2048$ and $X = 2048\,\mathrm{m}$ giving $k_{\min} = 0.003\,\mathrm{m}^{-1}$ and $k_{\max} = \pi\,\mathrm{m}^{-1}$.

For the Bradley case it is seen that $z_r \gg z_0$, remark that the length scales are shown in meter while z_0 is given in millimeter, but $z_r \ll l$ is not fulfilled. For more normal cases with a larger z_0 the ratio z_r / l shall be even larger as $z_r \propto z_0^{1/3}$ and $l \propto z_0^{1/6}$ approximately. This is clearly seen for the Peterson case.

In figures 2, 3, and 4, LINCOM calculations are compared to surface friction and velocity data of Bradley [3] and to velocity data of Peterson et al [9], all for each of the three models: a) $z_r = z_0$, b) $z_r = a\, z_{1,\max}$, and c) $z_r = 0.3\, z_0^{0.33}\, L^{0.67}$ with $a = 10$ for the Bradley case and 100 for the Peterson case. For all cases the fitting parameters c_1 and c_2 have been kept equal to 1.

It is quite clear from the figures that with $z_r = z_0$ the velocity perturbations are overpredicted and the friction velocity unperturbed. $z_r = 0.3\, z_0^{0.33}\, L^{0.67}$ is good in both tests. In the Bradley test both the friction and the velocities at low heights indicate that $z_r = 0.3\, z_0^{0.33}\, L^{0.67}$ is better than $z_r = 10\, z_{1,\max}$. The calculated velocity profiles better follow the abrupt trends of the data points and don't start changing so much in advance of the roughness change and U_* approaches the data better although it is still somewhat underpredicted after the smooth to rough transition. The delay – or downstream offset – of the calculated minimum velocity for the Bradley case is increasing with increasing height. It is smallest with $z_r = z_0$ and a little larger with the other two z_r's.
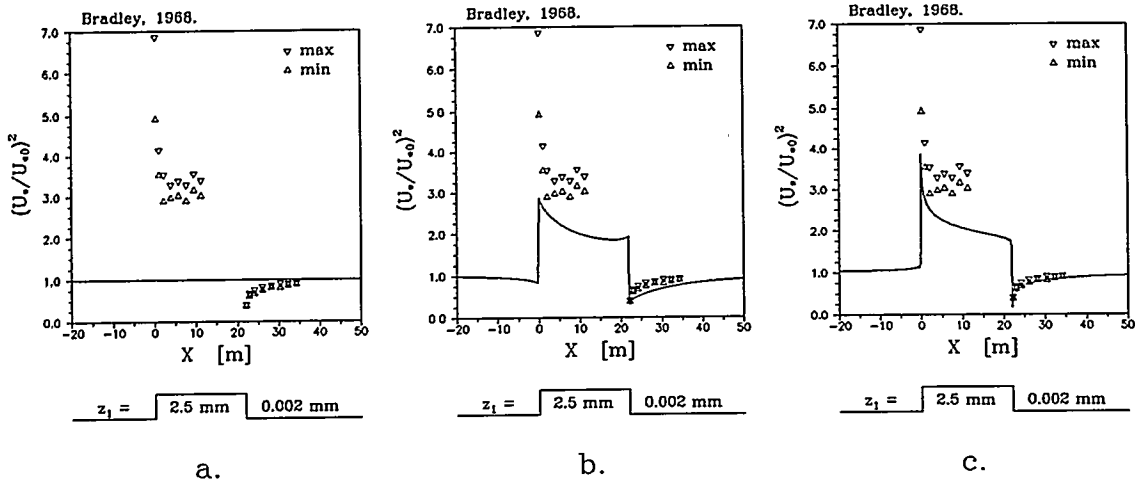
Figure 2. LINCOM calculations compared to friction data of Bradley [3].
a) $z_r = z_0$ b) $z_r = 10\, z_{1,\mathrm{max}} = 25\,\mathrm{mm}$ c) $z_r = 0.3\, z_0^{0.33}\, L^{0.67}$
Marks indicate measurements, solid lines calculations.

Not presented here are calculations in which the fitting parameter c_2 has been varied. While the c_1 parameter has been set to unity for all calculations, we have tried to combine $z_r = z_0$ with a value of c_2 less than one. $c_2 = 0.3$ gives reasonable results close to the ground but higher up the horizontal velocity profiles get too flat, ie the perturbations are underpredicted, and the delay in the calculated minimum velocity in the Bradley case gets much larger than for the cases presented in the figures.

7 Applications

7.1 The Askervein hill

The Askervein hill project is described in detail by Taylor and Teunissen [11], Mickle et al [7] and Salmon et al [6]. For the present 1D calculations the hill profile is taken as the Gaussian profile with which Zeman and Jensen [16] approximated the main profile of the real hill ie that perpendicular to the ridge line and through the hill top. With all units of lengths in [m] we have:

$$\widetilde{h} = 115 \exp\left[-\left(\frac{x}{225}\right)^2 \ln 2\right] \tag{94}$$

Based upon the measurements at the reference station a few miles upstream of the hill Zeman and Jensen found the surface roughness height there to be $z_0 = 0.03$ m. At the hill top it was clearly smaller and they found best correspondence between their model calculations and the data using the following roughness height profile:

$$z_1 = \begin{cases} 0.03 & \text{for } x \leq -225 \\ 0.01\left(1 + 2\exp\left[-4\left(1 + \dfrac{x}{225}\right)^2\right]\right) & \text{for } -225 \leq x \leq 0 \end{cases} \tag{95}$$
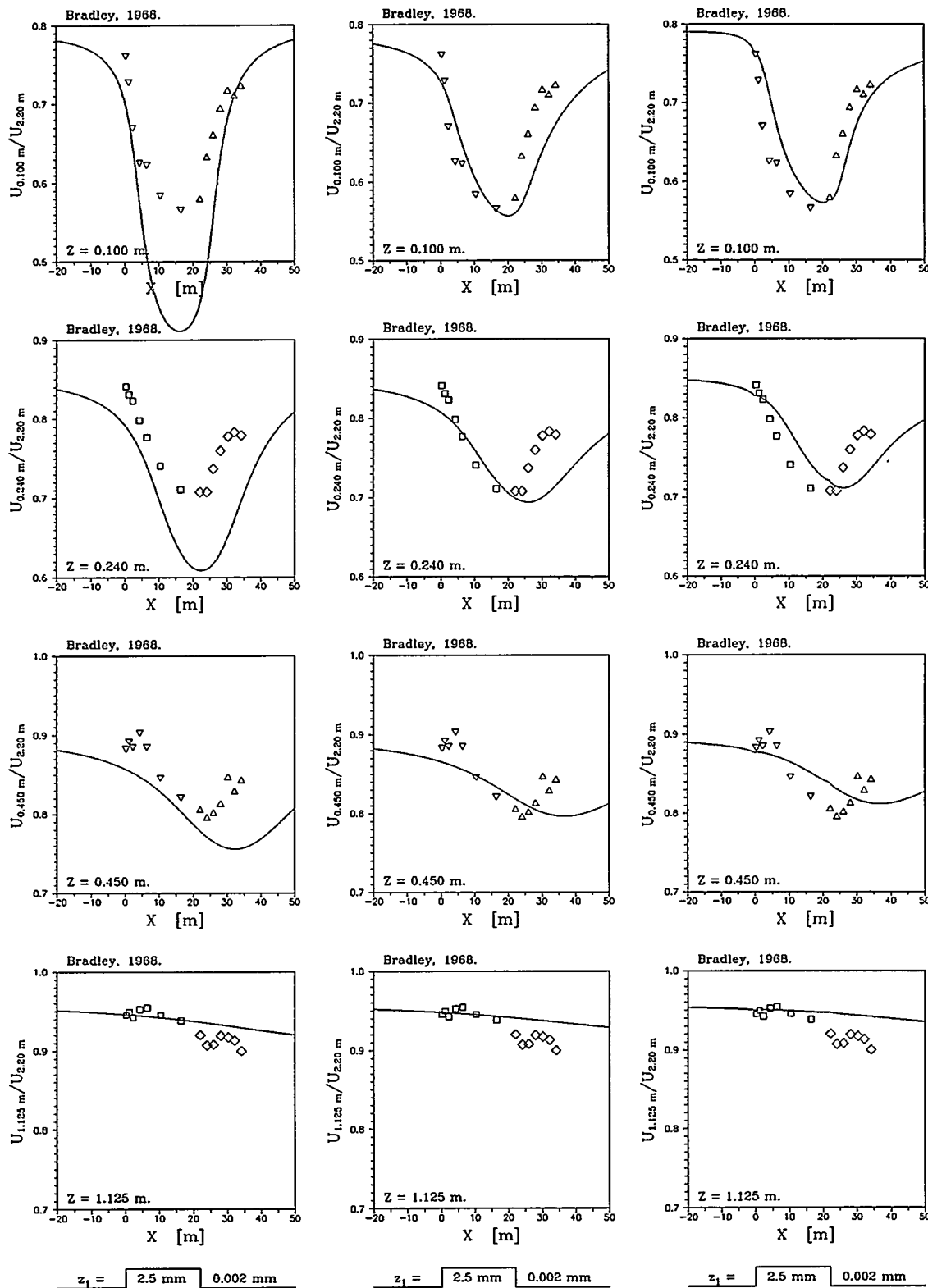
Figure 3. LINCOM calculations compared to velocity data of Bradley [3].
a) $z_r = z_0$ b) $z_r = 10 \, z_{1,\text{max}} = 25 \, \text{mm}$ c) $z_r = 0.3 \, z_0^{0.33} \, L^{0.67}$
Marks indicate measurements, solid lines calculations.
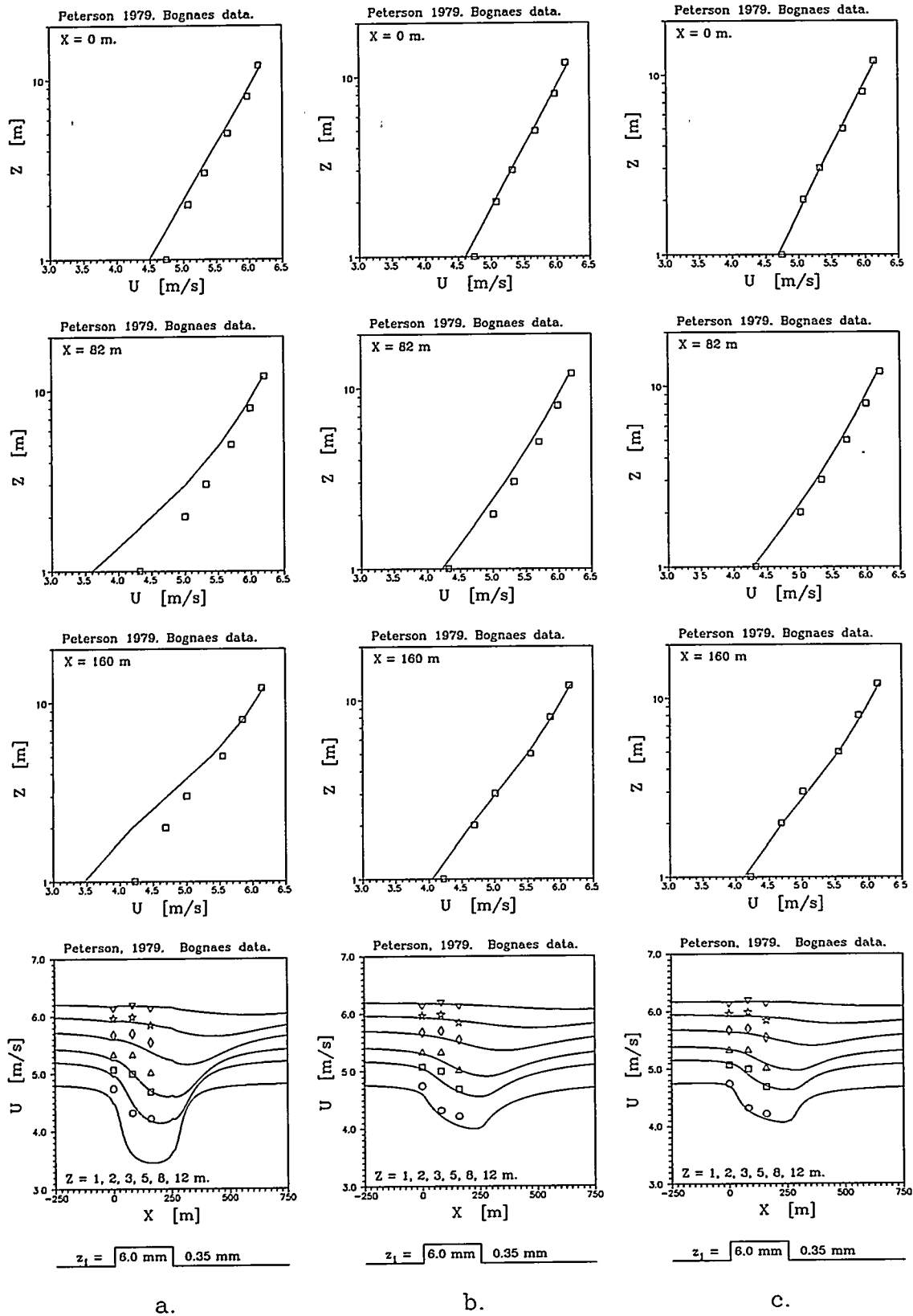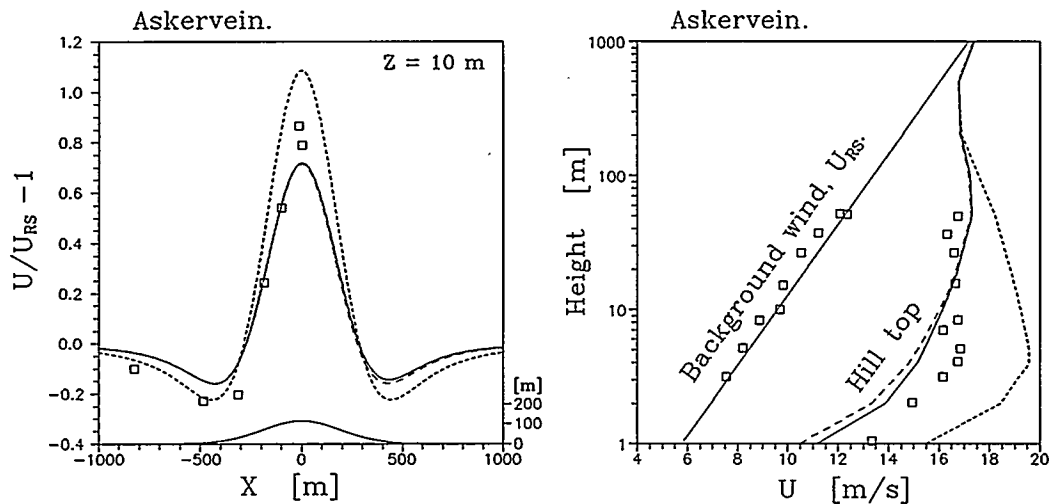
Figure 4. LINCOM calculations compared to velocity data of Peterson et al [9].
a) $z_r = z_0$ b) $z_r = 100\,z_{1,\max} = 600\,\mathrm{mm}$ c) $z_r = 0.3\,z_0^{0.33}\,L^{0.67}$
Marks indicate measurements, solid lines calculations.

Figure 5. Left: Horizontal profiles of relative wind speedup 10 m above ground plus hill profile. Right: Vertical profiles of wind speed. Squares indicate measurements. RS: Reference station. Calculations: Full line: varying roughness. Dashed line: constant roughness. Short dashed line: constant roughness and simpler approach of chapter 5.1.

where again all units of lengths are in [m]. The used wind data are from 3rd October 1983, 1430 to 1530 British summer time, where the mean wind direction was 210° ie almost in the main profile direction of roughly 43/223°. At the reference station the wind profile was then nearly logarithmic, the friction velocity being 0.66 m/s. That is used for the background flow in the LINCOM calculations.

Figure 5 compares the calculations to the measured data, which are here being reproduced from Zeman and Jensen [16]. Horizontal profiles of relative wind speedup at 10 m above the surface and vertical wind profiles at the hill top are presented for three different calculations: 1) the roughness height follows eq. 95, solid line, 2) constant roughness height $z_0 = 0.03$ m, dashed line, and 3) constant roughness height and application of the so called simpler approach described in chapter 5.1, short dashed line. The bottom curve in the horizontal profiles plot is the modelled hill profile, eq. 94.

At 10 m height the calculated velocities don't vary as much as measured except for the simpler approach (described in chapter 5.1) which overpredicts the variation slightly, and the hill top vertical profiles don't show the almost constant velocity above 4 m. But with the 1st order model concept of LINCOM in mind the results are all together surprisingly good.

7.2 North-Eastern Zealand

As a demonstration of the 2D capability, the velocity perturbation due to the surface roughness distribution has been calculated for an area covering the north-eastern part of Zealand, Denmark. The perturbations caused by the hills are not taken into account here.

The roughness pattern is described by four roughness categories: 1) sea and lakes

with $z_1 = 0.005$ m, 2) agricultural land with $z_1 = 0.05$ m, 3) urban ares with $z_1 = 1.0$ m, and 4) forests with $z_1 = 1.5$ m. With a resolution of 500 m the distribution of the four roughness elements are shown in figure 6. Some of the 'lakes' at that figure are actually part of a fjord.

The background wind is set to be in equilibrium with a surface roughness height of 0.005 m – the specified sea roughness height – when given a speed of 10 m/s at 20 m height. The wind direction is 300° ie 30° north of west.

Figures 7 and 8 are vector plots of the calculated perturbation velocities and of the total velocities, both at 1 m height. The contours of land and lakes are also shown. Held together with figure 6 the plots show the expected trends: large perturbations over urban and forest areas and no or next to no perturbations over sea and lakes.
When the wind close to the ground is slowed down at the high roughness spots the excess air has to raise or to escape sideways to areas with lower roughness. It does both but the perturbation component perpendicular to the background wind direction is small compared to the aligned component so the sideways escaping effect can not be seen on the plots.
Figure 9 shows a map of the surface friction velocity distribution, darker shade meaning higher friction. It is seen how U_* spikes positively at the smooth to rough transitions at the western edges of the high roughness regions and negatively at the rough to smooth transitions at the eastern edges, all in correspondence with the behaviour presented in figure 2 c.

8 Conclusion

Within the basic linearized concept of the LINCOM model for flow over complex terrain, this model has been successfully extended with a feature for including the influence of heterogeneous surface roughness. The main assumption of the new feature is that up to a certain reference height z_r, the flow is in equilibrium with the underlying local surface roughness. The value of z_r has a marked influence on the calculated perturbations, and not being analytically determinable it has had to be determined from scale arguments and comparisons to experiments. Operating in Fourier space, a formula for z_r as function of wavenumber has been found which makes calculated and measured velocity data correspond well for two well defined test cases, and which makes the calculated surface friction velocity follow the measured trends although the actual values are somewhat underpredicted at a smooth to rough transition.
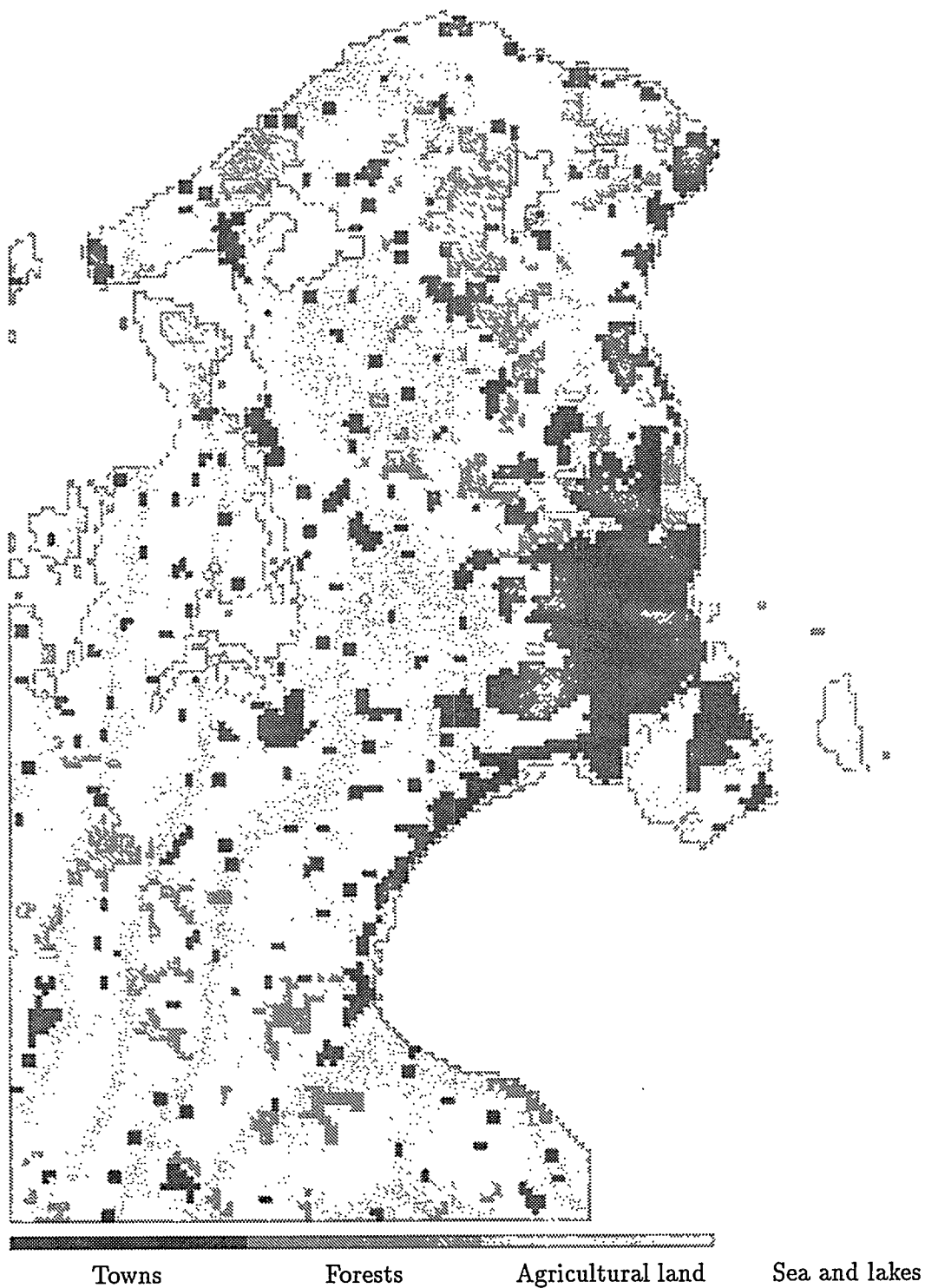
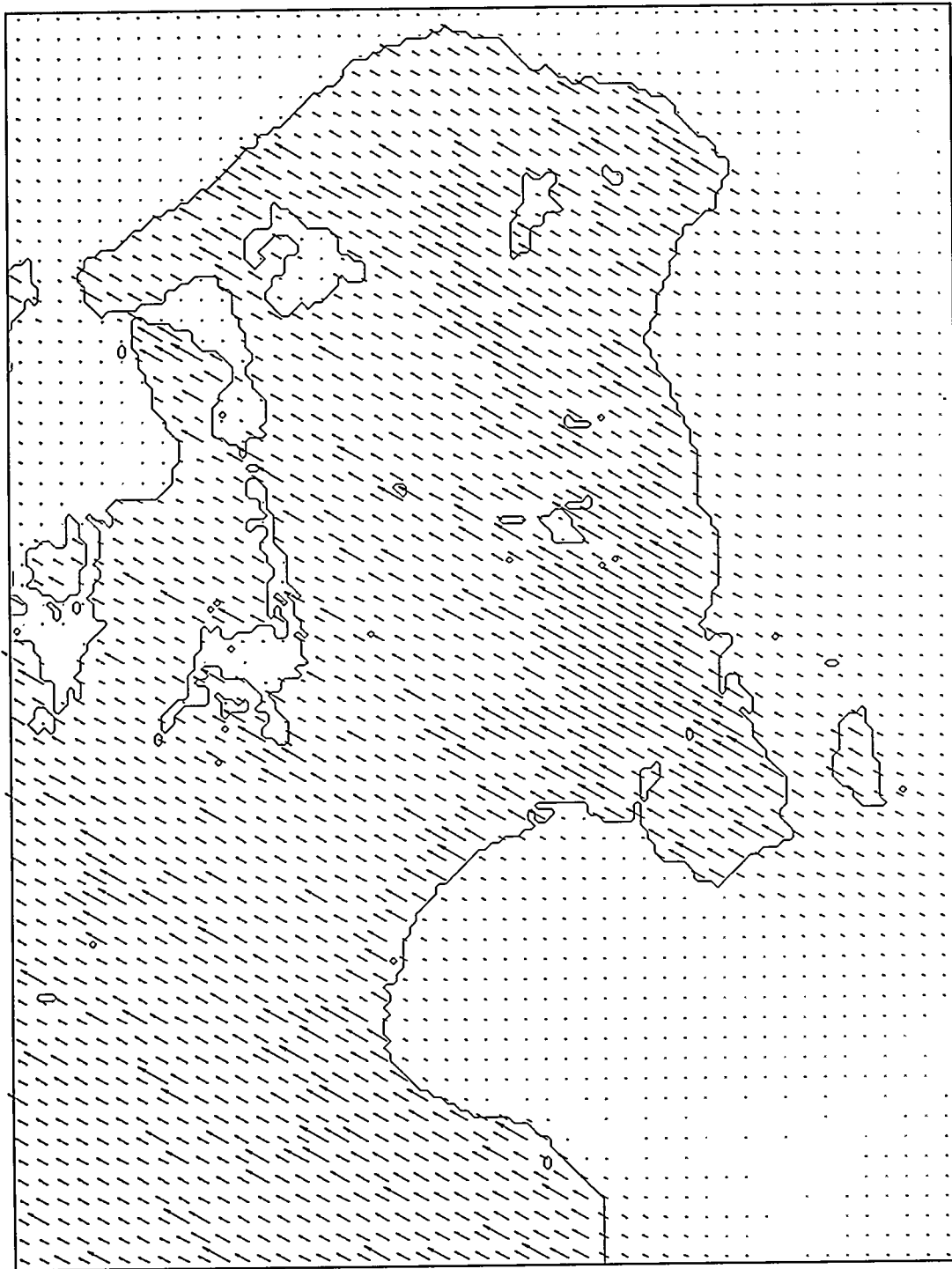**Figure 6.** Distribution of roughness elements in north eastern Zealand.

| Towns | Forests | Agricultural land | Sea and lakes |

Figure 7. Velocity perturbations vectors 1 m above ground.
Scale: ——— ≈ 10 m/s, ie 1 m/s per mm.
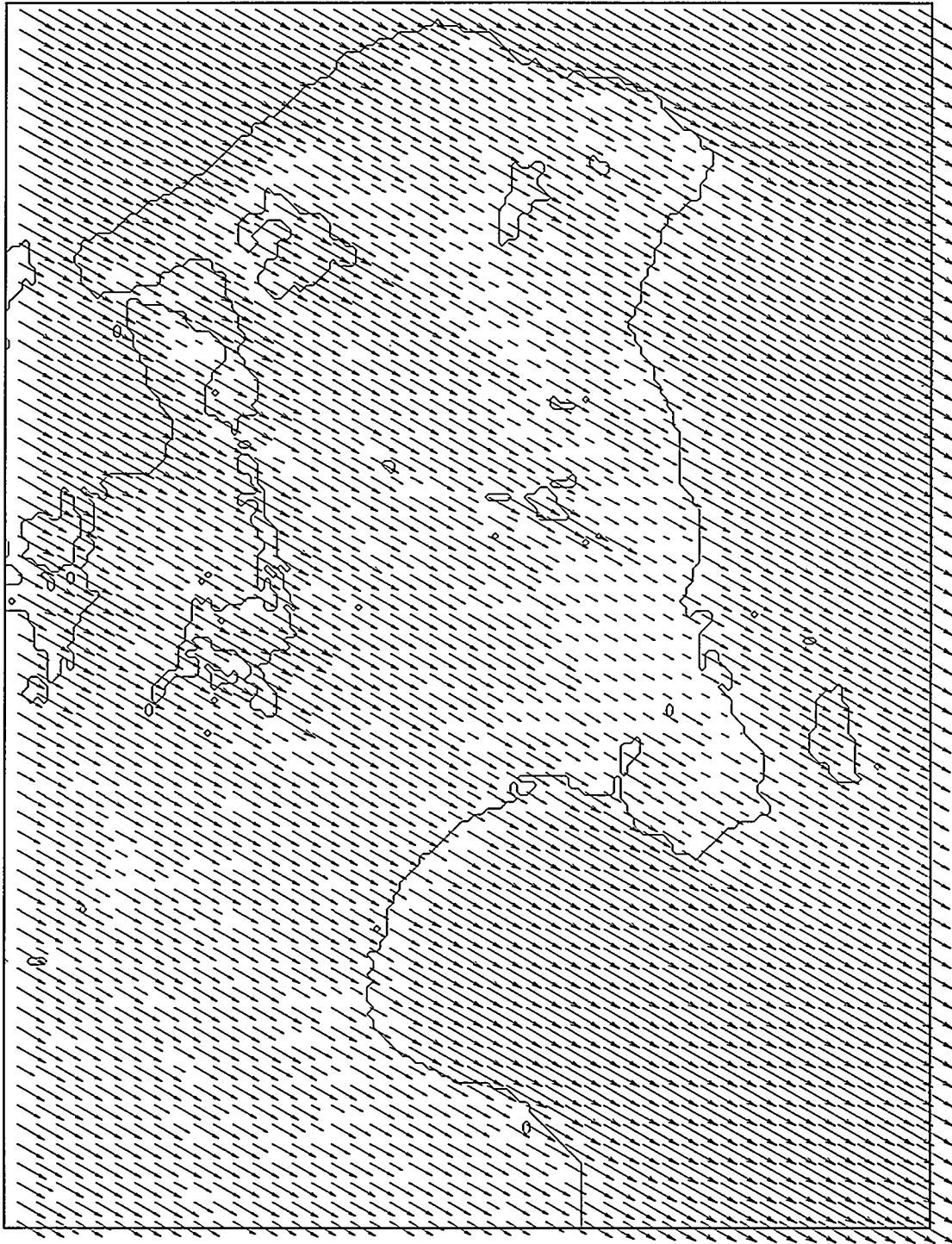
Figure 8. Wind velocity vectors 1 m above ground.
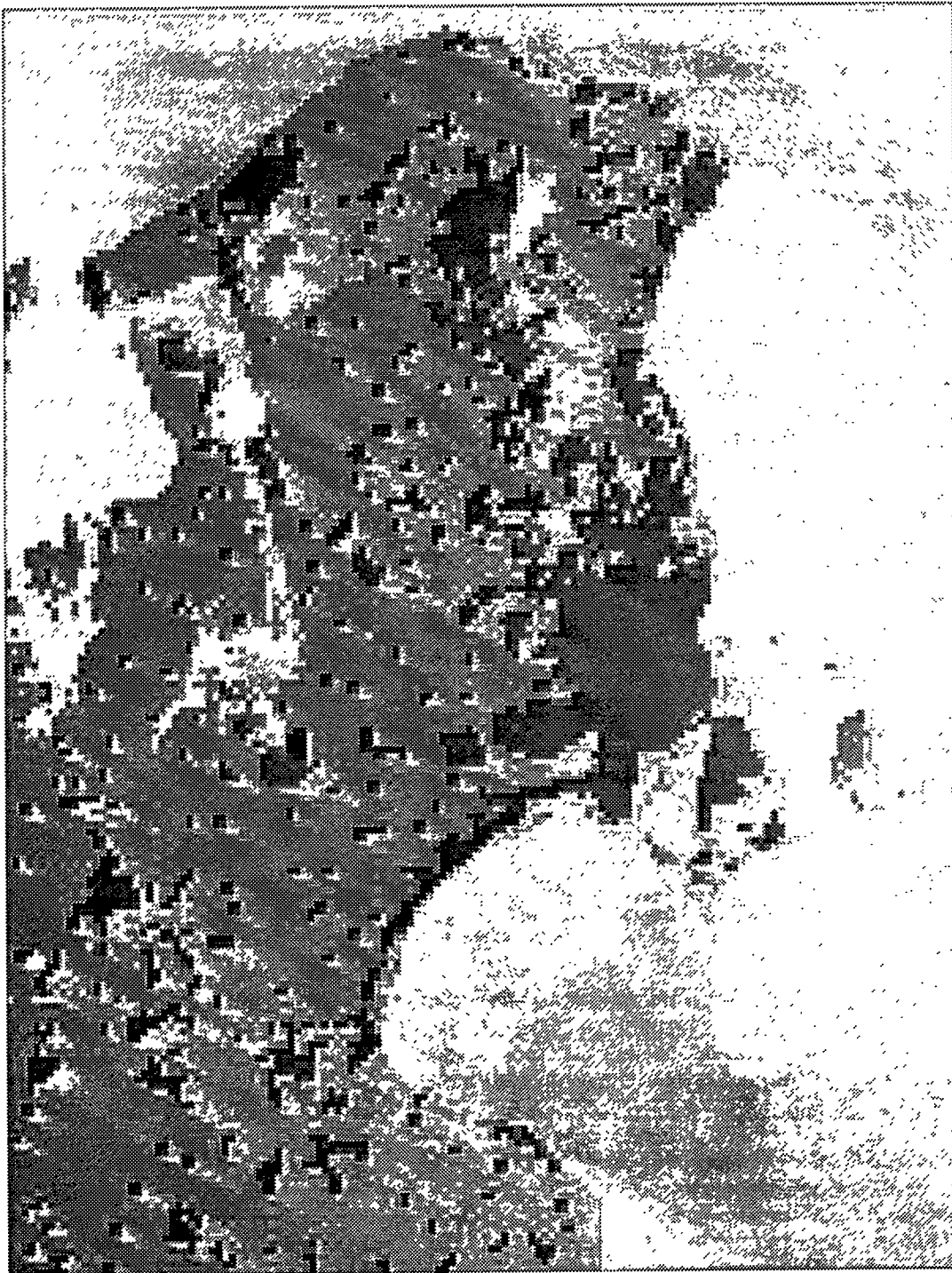Scale: ——— ≈ 10 m/s, ie 1 m/s per mm.

Figure 9. Surface friction velocity distribution. Darker means higher value.

References

[1] Astrup, Poul. *Turbulent Gas-Particle Flow.* Risø-R-618(EN). Risø National Laboratory, Denmark, 1992. Ph.D. thesis.

[2] Belcher, S.E.; Xu, D.P.; and Hunt, J.C.R. The response of a turbulent boundary layer to arbitrarily distributed two-dimensional roughness changes. *Quarterly Journal of the Royal Meteorological Society*, 116:611–635, 1990.

[3] Bradley, E.F. A micrometeorological study of velocity profiles and surface drag in the region modified by a change in surface roughness. *Quarterly Journal of the Royal Meteorological Society*, 94:361–379, 1968.

[4] Jackson, P.S. and Hunt, J.C.R. Turbulent wind flow over a low hill. *Quarterly Journal of the Royal Meteorological Society*, 101:929–955, 1975.

[5] Jensen, N.O.; Petersen, E.L.; and Troen, I. *Extrapolation of mean wind statistics with special regard to wind energy applications.* WCP-86. World Meteorological Organization, 1984. WMO/TD-No. 15.

[6] J.R.Salmon; Bowen, A.J.; Hoff, A.M.; Johnson, R.; Mickle, R.E.; P.A.Taylor; Tetzlaff, G.; and Walmsley, J.L. The Askervein Hill Project: Mean wind variations at fixed heights above ground. *Boundary-Layer Meteorology*, 43:247–271, 1988.

[7] Mickle, R.E.; Cook, N.J.; Hoff, A.M.; Jensen, N.O.; J.R.Salmon; P.A.Taylor; Tetzlaff, G.; and Teunissen, H.W. The Askervein Hill Project: Vertical profiles of wind and turbulence. *Boundary-Layer Meteorology*, 43:143–169, 1988.

[8] Mikkelsen, T.; Larsen, S.E.; and Thykier-Nielsen, S. Description of the risø puff diffusion model. *Nucl. Technol.*, 67:56–65, 1984.

[9] Peterson, Ernest W.; Jensen, Niels Otto; and Højstrup, Jørgen. Observations of downwind development of wind speed and variance profiles at Bognaes and comparison with theory. *Quarterly Journal of the Royal Meteorological Society*, 105:521–529, 1979.

[10] Santabàrbara, J.M.; Mikkelsen, T.; Kamada, R.; Lai, G.; and Sempreviva, A.M. *LINCOM. Wind flow model.* Risø National Laboratory, Denmark, 1994. Not published.

[11] Taylor, P.A. and Teunissen, H.W. The Askervein Hill Project: Overview and background data. *Boundary-Layer Meteorology*, 39:15–39, 1987.

[12] Troen, Ib. On diagnostic wind field models. 1990. Presented on the College on atmospheric boundary layer physics, 21 May 1990.

[13] Troen, Ib and de Baas, Anne. A spectral diagnostic model for wind flow simulation in complex terrain. In: *Proceedings of the European Wind Energy Association Conference & Exhibition*, pages 37–41. Rome, 1986.

[14] Troen, Ib and Petersen, Erik Lundtang. *European Wind Atlas.* Risø National Laboratory for the Commission of the European Community, 1989.

[15] Walmsley, J.L.; Taylor, P.A.; and Keith, T. A simple model of neutrally strat-
ified boundary-layer flow over complex terrain with surface roughness mod-
ulations (MS3DJH/3R). *Boundary-Layer Meteorology*, 36:157–186, 1986.

[16] Zeman, Otto and Jensen, Niels Otto. Modification of turbulence characteris-
tics in flow ower hills. *Quarterly Journal of the Royal Meteorological Society*,
113:55–80, 1987.

A Boundary Conditions

The solution for the Fourier transform of a perturbation is found analytically and consists of the sum of an outer and an inner solution as explained in chapter 4. The 'arbitrary' constants vectors for the inner and outer solutions contain together three independent parameters which have to be determined from three applicable boundary conditions. In principle all boundary conditions should be applied to the total solution, but when either the inner or the outer solution dominates, little error is introduced in applying the *main* boundary condition to the dominating solution and then use a secondary condition to adjust the total solution.

For flow over hills, Troen and de Baas [13] use scale arguments to show that the main boundary condition, which for this case states that the flow near the ground is parallel to the ground, can be applied to the inviscous outer solution separately, whereafter boundary conditions for the inner solution can be selected to give zero total horizontal velocity perturbations at ground level, see table 1.

For the roughness perturbations the main boundary condition is the velocity equilibrium with the local surface roughness in a layer close to the ground, and as the perturbation is assumed to be aligned with the background wind this gives two boundary conditions, one for each of the two horizontal velocity components. In this case the inner solution is dominating and these two conditions are applied to the inner solution only, whereafter a boundary condition for the outer solution is selected to give zero total vertical velocity perturbation at ground level, see table 1.

	Inner solution	Outer solution
Hill	$u_{z=0} = v_{z=0} = 0$	$\widetilde{w}_{1,z=0} = V_L \cdot \nabla \widetilde{h}$
Roughness	$\widetilde{v}_{z=z_r} = z_r \left. \dfrac{\partial \widetilde{v}}{\partial z} \right|_{z=z_r} \ln \dfrac{z_r}{z_0} - e \dfrac{U_{*0}}{\kappa} \ln \eta$	$w_{z=0} = 0$

Table 1. Applied boundary conditions.

Applying the boundary conditions to the inner and outer solutions separately makes it all more simple and not less accurate. The whole model anyway relies on first order approximations and the main boundary conditions are not well defined physical conditions but rather conditions derived from such using scale arguments.

Bibliographic Data Sheet

Title and author(s)

Surface Roughness Model for LINCOM

Poul Astrup, Niels Otto Jensen, and Torben Mikkelsen

Abstract (Max. 2000 char.)

The LINCOM model for neutrally stable flow over complex terrain, developed in 1986 by Troen and de Bass [13], has been extended to also respond to variations in surface roughness. The extension is based on the assumption that close to the ground the flow is in equilibrium with the local surface roughness, and on a model for the vertical extent of this equilibrium zone.

LINCOM is based on an analytical solution in Fourier space to a set of linear equations derived from the normal nonlinear mass and momentum equations for fluid flow. The linear equations describe the perturbations in velocity and pressure that the real terrain induces in an equilibrium flow corresponding to a flat terrain with uniform surface roughness. The perturbations caused by gradients in ground elevation and surface roughness are determined separately and summed as a first order approximation to the combined perturbation.

Descriptors INIS/EDB

BOUNDARY LEVELS; COMPLEX TERRAIN; FLOW MODELS; FOURIER TRANSFORMATION; L CODES; LEVELS; ROUGHNESS; STEADY FLOW